NASA-CR-204947

Study of a Solar X-Ray Telescope

FINAL
IN-89-CR
OCIT
034741

NASA Grant H-27835D

Final Report

For the Period 28 February 1997 through 30 May 1997

Principal Investigator
Dr. Leon Golub

May 1997

Prepared for:

National Aeronautics and Space Administration
Marshall Space Flight Center
Marshall Space Flight Center, AL 35812

Smithsonian Institution
Astrophysical Observatory
Cambridge, Massachusetts 02138

The Smithsonian Astrophysical Observatory
is a member of the
Harvard-Smithsonian Center for Astrophysics

The NASA Technical Officer for this grant is the New Technology Representative/LA10, National Aeronautics and Space Administration, Marshall Space Flight Center, AL 35812.

1.1 Overview

The highly structured nature of the outer solar atmosphere seems to be intimately linked to the presence, at the solar surface, of magnetic fields that have been generated inside the Sun and have emerged to the surface. The corona is brightest (and also hottest) at just those locations where magnetic field has emerged from inside the Sun. Dynamo theory predicts that strong magnetic fields will be generated deep in the solar interior and that bundles or "ropes" of magnetic flux will float to the surface. When this happens, a magnetically bipolar region will become visible, extending above the surface in a three-dimensional structure.The field lines penetrate through the surface, showing two magnetic poles, and also exhibit a three-dimensional structure above the surface.

The structure created by the field emergence is rooted in the (relatively) cool photosphere and extends through the chromosphere and transition region to the corona. Thus, the magnetic field creates a region, called an *active region*, which contains portions at temperatures from $< 10^4$ K to $> 10^6$ K, and is therefore visible at wavelengths from the infrared through x-rays. The locations where the magnetic field leaves and reenters the visible surface are called the "footpoints" of the coronal structures associated with the magnetic field.

The magnetic fields themselves are not directly visible. However, the hot coronal plasma is, for the most part, constrained to follow the direction of the magnetic field lines in the atmosphere. Now, 100 years after the discovery of x-rays by Wilhelm Roentgen in 1896, we can routinely make observations of the solar corona from outside the Earth's atmosphere in this region of the electromagnetic spectrum. As shown by comparing x-ray images with magnetograms, the bright corona over these bipolar magnetic regions consists of closed structures that seem to follow the orientation of the magnetic field. Although we can see down to the photosphere at x-ray wavelengths when observing on the disk of the Sun, this part of the solar atmosphere emits so little that far from the peak of its Planck curve that it appears dark in x-ray images. This impression of hot plasma following the magnetic field direction is further strengthened by quantitative studies that calculate coronal

Contents

magnetic field strength and direction based on photospheric measurements[1] and compare them with the observed brightness and location of the x-ray emitting structures. Such comparisons make it clear that, for the most part, the hot plasma conforms to the geometry of the magnetic field and that the coronal brightness is strongly linked to the strength of the magnetic fields which have erupted to the solar surface from the interior. It is also the case that the larger-scale, fainter corona, as well as coronal holes, are strongly influenced by the large-scale solar magnetic field.

We may get a small hint of the reason that the coronal plasma outlines the direction of **B** by examining the thermal conductivity of a hot plasma in the presence of a magnetic field. This quantity has enormously different values in the directions parallel and perpendicular to the field (see e.g. Spitzer, 1962): for a coronal temperature of 10^6 K, a particle density of 10^9 cm^{-3} and a magnetic field strength of 100 G, the conductivity along the field is approximately 13 orders of magnitude greater than that perpendicular to the field. It is therefore not surprising that a parcel of plasma which is locally heated would conduct that heat preferentially in the direction of the field. We also note that the thermal conductivity parallel to the magnetic field *increases* with temperature T, while the perdendicular conductivity *decreases.* To the extent that the loop *aspect ratio*, i.e., the ratio of loop length to loop width, is determined by the thermal conductivity, we would expect that higher temperature loops are longer and thinner than cooler ones. However, if the loop width becomes smaller than the spatial resolution of the observing instrument, this effect will not be directly observable.

For organizational purposes, on the next page we provide a listing of some scientific objectives for a Solar-B x-ray telescope, arranged in terms of identifiable features in the corona.

[1]Note that no reliable method for measuring coronal magnetic field strengths directly has yet been developed.

Solar-B X-ray Telescope

Science Objectives by Topic:

I. Small-scale Structures in the Solar Corona

II. Temperature Structure of the Corona

III. Velocity Fields in the Corona

Science Objectives by Feature:

I. AR Structure and Variability

1. Temperature Structure
2. Loop Static Fine Structure
3. Loop Dynamics – variability and flows

II. Coronal Holes: Formation and evolution

III. Large-scale structure

a. Interconnecting loops.

b. Outside of ARs – relation to large-scale dynamics

c. Polar plumes

d. Corona above and around sunspots

IV. Filaments and Prominences: Formation and Activity

V. "Transition Corona" (inner to outer corona)

– mass, momentum & energy transfer

VI. Flares: Reconnection, Microflares, Nanoflares & Jets

VII. CMEs & Coronal Transients

VIII. XBP: Structure, evolution and dynamics

2.1 GI *vs.* NI Telescopes

In order to discuss the relative merits of grazing-incidence (GI) *vs.* normal incidence (NI) x-ray telescopes, it is first necessary to consider the nature of the coronal emission. Comparison of the coronal emission to the instrumental capabilities can then be carried out, in order to determine the pros and cons of the two techniques.

2.1.1 Plasma diagnostics

Because of the high coronal temperature, the radiative output is primarily in the form of emission lines of highly excited ions of heavy elements, such as Fe, Si, Mg, etc. Continuum emission is also present, although at a low level for portions of the corona below flare temperature (10^7 K). Although some coronal lines are emitted in the visible and even the IR, the strongest lines are in the XUV and soft x-ray region of the spectrum.

In order to carry out diagnostics of the coronal plasma, the isolation of a single spectral line is preferable, although this work can also be done if the observed emission is dominated by only a small number of spectral lines. Obtaining a narrow slice of a broadband spectrum always involves a reflection and a transmission, so that both the long and the short wavelength ends can be eliminated. Thus x-ray telescopes require transmission filters as well as reflective optics.

Techniques for analyzing GI data ("broadband" images) have long been known (e.g., Vaiana *et al.,* 1973) and will not be described here. Techniques for utilizing the newer x-ray multilayer optics, operating at near-normal incidence, are not as well known and will be described in some detail here. The discussion involves three steps: i) we list the strongest emission lines in the solar spectrum, ii) we limit our study to the range of wavelengths for which multilayers might conceivably be used; this is taken to be 17–335 Å, and iii) specific consideration is given to those lines which would provide unambiguous diagnostice over the full range of temperatures from the chromosphere through flares ($10^4 - 10^{7.5}$ K). The lines which we have included in the present study are listed in Table 2.1.

Table 2.1: Soft x-ray and XUV lines included in this study.

Species	Wavelength (Å)	$\log(T_{max})$
Fe XX	12.8 – 13.0	7.0
Fe XIX	13.5	6.9
Fe XVIII	14.1 – 14.6	6.8
Fe XVII	15.0 – 15.5, 16.78 – 17.10	6.6
O VIII	18.97	6.5
O VII	21.60, 21.81, 22.10	6.3
C VI	33.74	6.1
Si XII	45.52, 45.68	6.3
Si XI	49.22	6.2
Mg X	57.9	6.1
Ne VIII	88.08	5.8
Fe XVIII	93.93, 103.95	6.8
Ne VIII	98.26	5.8
Ne VII	115.52, 116.69	5.7
Fe XXII	116.29, 117.17	7.1
Fe IX	171.07	6.0
O V	172.17	5.4
O VI	172.94, 173.08	5.5
Fe X	174.53, 177.24	6.1
Fe XI	180.41, 182.17, 188.22	6.2
O VI	183.95, 184.13	5.5
Fe XXIV	192.03	7.3
Fe XII	192.40, 193.52, 195.13	6.2
Fe XIV	211.32, 274.24	6.2
He II	256.37	4.6
Fe XV	284.16	6.3
He II	303.79	4.6
Si XI	303.33	6.2
Fe XVI	335.40	6.4

Examination of the lines available to NI telescopes ($\approx 44 - 400$ Å) shows the main limitation of multilayers as a diagnostic tool. Differential emission measure analyses (e.g., Brosius *et al.*, 1996) show that the large-scale, or "quiet" corona, has most of its emission measure at log T=6.0–6.3, and these temperatures are covered quite well by the spectral lines available to NI telescopes. However, active regions have their peak DEM in the range log T=6.5–6.8, a region that is best observed in O VIII and FE XVII. However, these lines are not available to present-day NI multilayer telescopes.

However, the spectral lines which are available to NI telescopes include the series of ionization stages of Fe from Fe IX through Fe XVI, inclusive. One can therefore observe *all* of the plasma in the temperature range log T=5.9–6.4 unambiguously. Since all of the stages are seen, the plasma has "nowhere to hide," and since the lines are all emitted by the same element, there are no abundances differences to worry about.

It may also be necessary to consider the atomic physics of line formation, for observations of rapid variability. As discussed in Golub *et al.* (1989), the ionization and recombination timescales for some ions are such that the observable changes may be limited by the line formation, rather than by the physical process responsible for the heating or cooling of the coronal plasma. For instance, the ionization timescale for the formation of O^{+7} is 230 seconds, whereas for O^{+6} the time is only 0.4 sec. Thus the ability to choose O VII rather than O VIII for a particular observation will make short timescale variability more easily detectable. In the other direction, the recombination time for Mg X under quiet corona conditions is 4×10^4 sec, whereas that for Fe X is only 500 sec; therefore the former line may become "frozen-in" under conditions of rapid cooling, should they occur. In any case, Fe X is preferable for observing rapid variability.

2.1.2 Image quality

The earliest x-ray images of the Sun were obtained using pinhole cameras (Blake *et al.*, 1963). Sounding rocket flights using transmitting zone plates were moderately successful (Einighammer *et al.*, 1967), but suffer from the problem that different wavelengths are focussed at different distances from the plate (chromatic aberration). An analysis of grazing-incidence systems, in which x-rays are reflected from the inside of a cylindrical surface via total *external* reflection was carried out by Wolter (1952a,b). Giacconi & Rossi (1960) proposed the use of such mirrors for x-ray astronomy, and by the mid-1960s several sounding rocket flights using such optics had proven their usefulness (Giacconi *et al.*, 1965; Underwood & Muney, 1967).

By applying Snell's law, we find that the critical angle for total external reflection is given by

$$\cos\theta_c \;=\; n. \tag{2.1}$$

If the imaginary part of n is small, then the critical angle is given approximately by $1 - \frac{1}{2}\theta_c^2 = 1 - \delta$, so that

$$\theta_c \;=\; (2\delta)^{1/2}, \tag{2.2}$$

or,

$$\delta \approx \frac{r_0}{2\pi}\lambda^2 n_e \;=\; \frac{r_0}{2\pi}\lambda^2 n_a\, f. \tag{2.3}$$

Note that θ_c turns out to be linearly proportional to the wavelength of the incoming x-rays. This means that at shorter wavelengths, or higher energies, the angle of reflection becomes smaller. For example, a grazing-incidence mirror made of, or coated with, beryllium will reflect 0.5 keV x-rays at angles up to 3°. The same mirror will reflect 3 keV x-rays only at angles less than about 30 arcmin, or 1/2°.

The rapid development of fabrication techniques for GI optics led to image quality ofabout an arcsecond by 1973. In addition to this improvement in image sharpness, or *accutance*, the amount of scattering was also greatly reduced in the more recent telescopes. Scattering is an especially severe problem in grazing-incidence telescopes, because the effects of surface roughness are greatly magnified by the small angle of incidence of the incoming rays. We note that in the more than two decades since 1973 improvements in surface smoothness have continued, as shown by the high quality of the *Yohkoh* SXT optics, and culminating in the remarkable quality of the *AXAF* mirrors (Van Speybroeck *et al.*, 1989), scheduled for launch in late 1998.

The normal-incidence (NI) reflectivity R of all materials in the soft x-ray/XUV region is a rapidly decreasing function of wavelength λ, with $R \propto$

λ^4. Thus, at 50 Å, for example, normal-incidence reflectivities no better than 10^{-5} are achievable from a single surface. However, by using multilayer coatings it is theoretically possible to enhance the normal-incidence reflectivity into the 30–70% range at wavelengths from 10–350 Å (Spiller *et al.*, 1980). This enhancement is not yet achievable in practice at the shorter wavelengths, but reflectivities near the theoretical values have been attained at XUV wavelengths in the 130–200 Å region (Barbee, 1986).

The normal-incidence reflectivity of a multilayer coating is relatively narrow band, where the bandwidth $\Delta\lambda/\lambda$ is approximately equal to $1/N_{lp}$, where N_{lp} is the number of layer-pairs (absorber–spacer) which contribute to the diffracted signal. At the same time, the signal, relative to that of a single-surface reflection, increases as N_{lp}^2. Thus, as more layers are deposited, the reflectivity curve becomes higher and narrower, until a limit resulting from absorption effects is reached.

The spatial resolution of optical instruments is generally limited by diffraction. At visible-light wavelengths, it has been possible to fabricate diffraction-limited optics for more than a century, and at soft x-ray wavelengths it is now possible to make telescopes operating at wavelengths 100 times shorter than visible light. Thus, the possibility exists that modest-size instruments could have resolutions of 0.01 arcsec or better.

However, the production of such instruments poses severe technical challenges. In general, our ability to fabricate mirrors has been determined by the measuring capability of our test instruments, i.e., by the mirror-makers' ability to know how well they have succeeded in figuring and polishing the surface during the fabrication process. Surface characterization capabilities have advanced considerably in recent years (see Spiller *et al.*, 1991 for a summary), so that figure qualities of 0.01 arcsec can now be measured. In principle, this means that the required surface quality is achievable, perhaps through a combination of standard optical polishing methods and final correction of the surface figure by the coating deposition itself. Fabrication of the *TRACE* optics shows that this can be done to the level of $\lambda/100$ for a 30 cm diameter mirror, which is more than adequate to provide that instrument's 0.5 arcsec resolution.

Finally, it is also necessary to consider the number of photons collected by the optics, since the photometric accuracy of the measurements is determined to some extent by counting statistics.[2] We may take as a baseline the requirement that an image contain 1000 counts per pixel as a definition of "photometric quality," although an image with 100 counts per pixel (average) will appear acceptable to the eye. One may then calculate, for the emission lines of the solar corona, what the resolution limit is for a large x-ray mirror, by working backwards from the assumption of 10^3 counts per pixel to an equivalent resolution value for a given set of physical limitations. The latter include: (a) a maximum exposure time, since the coronal dynamics are likely to produce changes or motions in the observed features, especially on the small spatial scales under consideration; (b) the strength of the emission lines in the corona, which determines the incident flux at 1 A.U.; and (c) the maximum practical mirror size, the transmissions of the necessary filters and the multilayer reflectivities at the various wavelengths, which determine the geometric and effective collecting areas available. Some other factors, such as detector resolution and efficiency, are omitted for simplicity in this discussion.

A summary of the limiting resolutions for some strong soft x-ray and XUV coronal emission lines is shown in Table 2.2. We have assumed a one-meter diameter mirror, one-minute exposure time, and have taken into account the approximate filling factor on the Sun for the emission. Thus, a high-temperature ion, such as Fe XVI, is emitted from a smaller volume of the corona than is a cooler ion such as Fe IX. A given value of the line intensity at 1 A.U. therefore implies brighter emission in, e.g., Fe XVI than in Fe IX *in those pixels which contain counts.* Defined in this way, the filling factor (*ff*) varies considerably as a function of temperature, and there may be an additional component to *ff* if there is substructure within the region under investigation.

The table also includes the variation as a function of wavelength of the assumed light-blocking filters. The values assumed for multilayer reflectivity

[2]It is perhaps a bit unusual to think of photon flux as affecting the resolution, but we are also requiring that the recorded data be of photometric quality.

Table 2.2: Countrate-limited spatial resolution values for some prominent coronal XUV emission lines.

Ion	λ (Å)	Flux[1]	$\log T_m^2$	filling factor	R_m^3	T_{fil}^4	Counts[5]	Resolution (arcsec)
Fe XVII	17.1	4×10^{-2}	6.6	0.04	0.02	0.8	4×10^5	0.05
Si XI	49.2	4×10^{-3}	6.2	0.05	0.10	0.5	1×10^5	0.10
Fe XVI	50.4	2×10^{-3}	6.4	0.05	–	–	–	–
+Si X	50.7	8×10^{-3}	6.1	0.75	0.10	0.5	5×10^4	0.14
Fe IX	171	7×10^{-2}	5.9	0.90	0.55	0.6	2×10^6	0.02
Fe XII	195	5×10^{-2}	6.2	0.70	0.50	0.6	2×10^6	0.02
Fe XV	284	4×10^{-2}	6.4	0.10	0.25	0.5	7×10^6	0.01
Fe XVI	335	2×10^{-2}	6.5	0.05	0.25	0.4	6×10^6	0.01

1. Typical full-disk value, in erg $\mathrm{cm}^{-2}\,\mathrm{s}^{-1}$, measured at the telescope entrance aperture.
2. Temperature of maximum formation of the line.
3. Fraction of the disk occupied by regions emitting the line.
4. Filter transmission at the wavelength of the line.
5. Average number of photons per arcsec^2 in one minute, without taking into account possible substructure.

(R_m) vary as a function of wavelength, from only a few percent at soft x-ray wavelengths to over 50% in the XUV.

The conclusion from such studies is that coronal imaging systems with a spatial resolution of 0.01 arcsec can be built, although with considerable difficulty. This is a factor of ≈ 100 better than has been achieved to date.

2.1.3 Countrate and Implications for Detector

As shown in Table 2.2, the countrates for typical bright coronal features are of order $10^4 - 10^6$ photons per arcsec^2 per sec. The sizescale of a typical active region in the corona is $\sim 100 \times 100 = 10^4$ arcsec^2, and many coronal brightenings are substantially larger, making the countrate at least 10^8 photons persec. However, heated material will often leave the initial location, or cause an event at a distant location. In practice full Sun image is therefore a necessity for studying coronal dynamics.

For countrate definition, we must also consider timescales of change for the object under study. Coronal cariability occurs on timescales of minutes, and may sometimes occur in a few seconds. Based on study of SXT, NIXT and EIT data, an image cadence of 100 seconds may be taken as the minimum needed for adequate detection and study of coronal events. This means that one must collect *at least* $10^6 - 10^9$ photons per second in order to study transient events in the corona.

Such countrate capabilites are far beyond the range of photon-counting imaging devices. Thus an integrating device must be used. In addition, today's state-of-the-art requires a spatial resolution exceeding that of previous experiments, such as the *Yohkoh* SXT and the *SOHO* EIT, which have ≈ 2.4 arcsec pixel size (5 arcsec resolution). A pixel size of 0.5 arcsec would match that of TRACE, which is the highest resolution coronal imager built to date. However, at this resolution, a full-Sun imager would need 4000×4000 pixels, thereby posing enormous data handling and processing costs on the experiment. An intermediate possibility, which would provide full-Sun imaging while representing a major advance over SXT and EIT would be to use a 2000×2000 pixel detector, with a pixel size of 1 arcsec.

3.1 Representative x-ray telescope designs

In this section we describe a number of telescope designs which might be considered for the coronal imaging instrument on Solar-B. We show five designs, which address the (sometimes conflicting) requirements of Solar-B:

1. Broad temperature coverage, with temperature diagnostic capability.

2. Full Sun field of view.

3. High spatial resolution.

In addition to the standard grazing-incidence (GI, Fig. 3.1) and normal incidence (NI, Fig. 3.2) telescopes, we also show the new tunable x-ray imager (TXI, Fig. 3.3) concept. We also indicate several combination instruments: an NI with both high resolution field-of-view and full Sun capability (Fig. 3.4) and a combined GI/NI telescope which gives both high resolution and full Sun as well as high and low temperature diagnostics (Fig. 3.5). It is also possible to build a tuneable grazing-incidence telescope, which utilizes a narrowband tuning mechanism rather than a filter wheel (Fig 3.6. For each design, we provide comments discussing the advantages and disadvantages from the point of view of the Solar-B science.

We note that the GI, NI and TXI instruments can, for costing purposes, be treated generically in the remainder of this document: they all contain x-ray optics, a structure, a mechanism and a detector; the NI and TXI designs may have a focal plane filter wheel, but this is not an absolute necessity. Our cost analysis in the next section of this report will be based on a grazing-incidence telescope, in order to have a specific instrument in mind when carrying out the design study and because it is likely to be the least expensive option. We note also that the combination instruments, while having greater scientific capability, will be more expensive because they contain additional optics and an additional mechanism.

3.1.1 Grazing-incidence telescope

The main advantage of the GI design is that it enables observation of the short-wavelength region below 44Å. Thus, the crucial coronal emission lines in the 10–20Å region can be observed, providing temperature diagnostics at 3–5 MK. Also, incoming photons are more energetic than in the XUV designs, so that detector efficiencies are generally higher, and surface contamination of mirrors, filters and detectors is less of a concern.

Temperature sensitivity in the 2 MK region is generally poor, but the instrument can be designed to emphasize this region. Options for accomplishing this are: choice of grazing angle, mirror coating material, use of thin filters, and use of a back-illuminated CCD.

The main disadvantage of GI telescopes is that, for Wolter I designs, the effective focal length is shorter than the physical length of the instrument. It is therefore difficult to obtain large plate scales for high (sub-arcsecond) imaging. Temperature diagnostics are obtained by inserting thin filters in the light path, which restricts the passband to a more or less narrow spectral region. For some designs, at certain plasma temperatures, the image may be dominated by a single ion; however, in general the images are formed by a combination of several strong spectral lines, and temperature diagnostics become complicated.

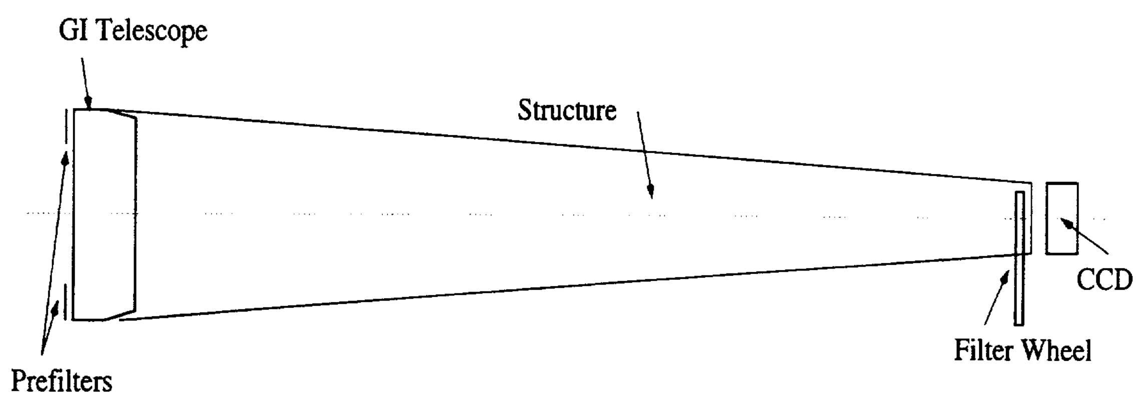

Figure 3.1: Schematic design of a typical grazing-incidence x-ray telescope.

3.1.2 Normal-incidence telescope

Normal incidence soft x-ray telescopes, which work by having special multilayer coatings applied to the optic, have two major advantages over GI telescopes: 1) the multilayer reflectivity is relatively narrowband, so that only one emission line, or only a few, can be selected; 2) operating at normal incidence, the image quality can be substantially better than that of a comparably-priced GI telescope. In particular, the region starting at 171Å contains a series of high-excitation lines of iron, from Fe IX up to Fe XVI, which provide excellent diagnostics for coronal plasmas.

The main disadvantage of NI telescopes is that they do not yet operate at short wavelengths, i.e., below about 44Å. Therefore, the very important emission lines of Fe XVII are not available, so that the temperature range 3–5MK is not well represented. O VII and O VIII are also not available in the XUV multilayer regime, although this is somewhat less of a problem. In addition, in most (but not all) multilayer designs, a different telescope is needed for each passband.

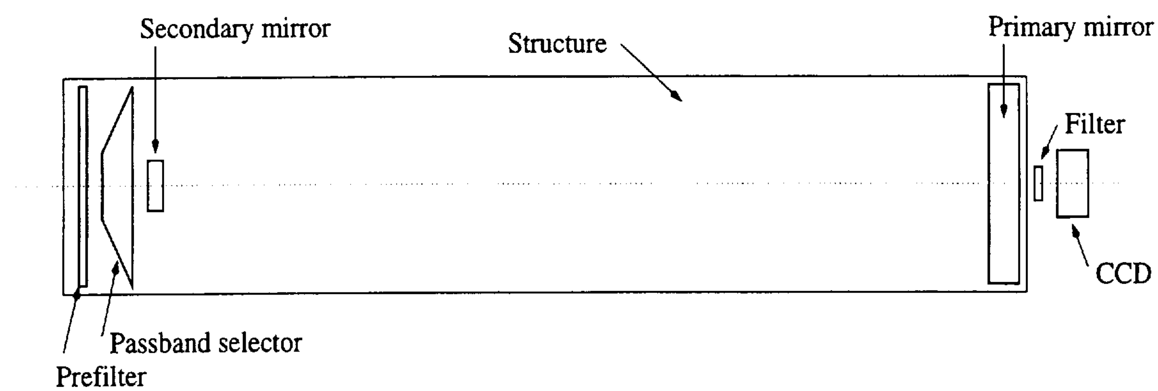

Figure 3.2: Schematic design of the strawman Solar-B normal incidence x-ray telescope.

3.1.3 Tuneable XUV imager

The Tuneable XUV Imager (TXI) is a variant of the NI design, since it uses XUV multilayer coatings to achieve high reflectivity. A fairly wide range of operating wavelengths is possible, from $\sim$ 44 Å to $\sim$ 400 Å. The essence of the design is to produce a broadband focussing mirror and to then have a double-crystal monochromator in the path to select a variable narrow wavelength band within the broader range. The monochromator uses two flat mirrors, parallel to each other, and arrangements with a fixed entrance and fixed exit beam path are possible, so that there is no image motion in the focal plane as the wavelength tuning is carried out.

The main advantage of this design over the standard NI is that *all* of the spectral lines within the broad passband can be selected, rather than just a few. In addition, the monochromator can be tuned on either side of the chosen line, and the difference image provides a velocity map of the corona in that line. Finally, if the monochromator is operated near the Brewster angle, only one sense of liner polarization is passed. Therefore, a 90-degree rotation of the instrument about the line of sight provides a polarization map of the corona in the line being observed.

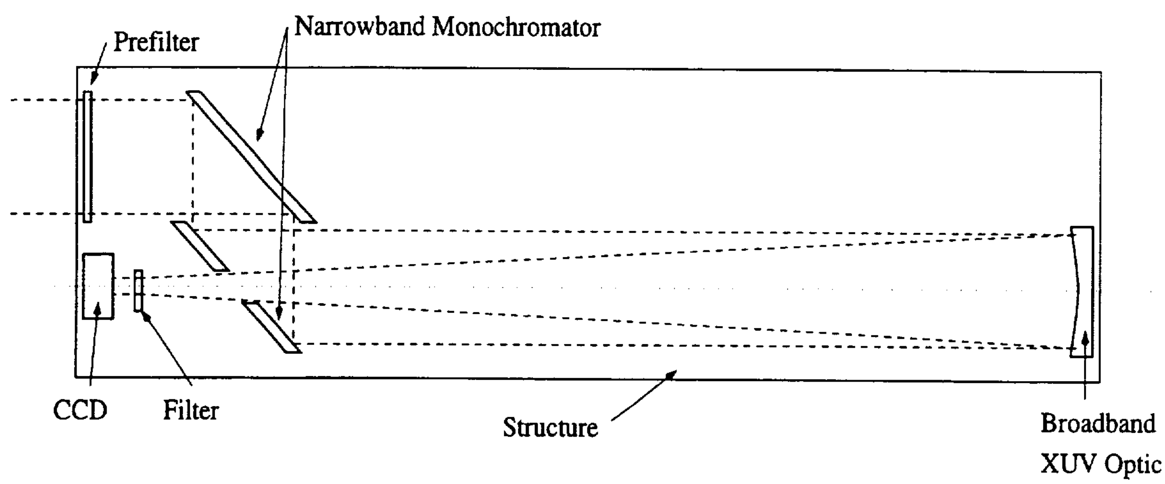

Figure 3.3: Schematic design of the tunable x-ray imager telescope.

3.1.4 Dual–scale NI imager

A major difficulty with the NI telescope is that, if it used for high resolution imaging, it will not be full Sun. In a ground-based optical telescope a change of magnification can be accomplished by switching eyepieces. This cannot be done in the XUV. However, in a Cassegrain design, it is possible to have a telescope in which the *secondary mirror* is changed. This can be done, for instance, by using a simple mechanism that inserts a flat mirror into the field, such that the primary mirror's beam is folded back to the focal plane; it is then equivalent to a prime-focus instrument. The positioning tolerance on the flat secondary is greater than on the magnifying secondary, so that the mechanism does not need to be extremely precise.

The advantage of this dual-scale design is that we can have a high resolution telescope, with e.g., 0.5 arcsec pixels, and a full Sun telescope with e.g., 2.5 arcsec pixels. The prime-focus mode would also have greater intensity per pixel, allowing the faint outer corona to be recorded.

The disadvantages of this design are, the increased complexity and risk due to the additional mechanism, and lack of high-temperature coverage common to all of the NI designs.

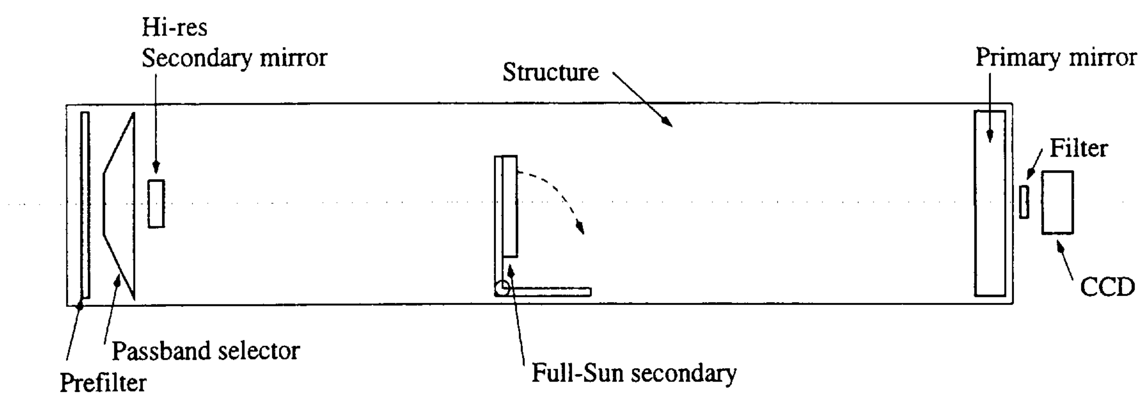

Figure 3.4: Schematic design of the dual-scale NI x-ray imager telescope.

3.1.5 Combination GI/NI x-ray telescope

As discussed above, one of the major difficulties in choosing between the GI and NI telescopes is that, with respect to temperature diagnostics of the coronal plasma, the two techniques are largely complementary. GI telescopes favor the higher temperature plasma above 2MK, while NI telescopes favor the lower temperature plasma below 2.5MK. There are a few possible emission lines at >5MK (such as Fe XVIII at 93.9 Å) that can be considered for

NI telescopes, but the important lines of Fe XVII, O VII and O VIII are not presently accessible.

It is therefore necessary to consider telescope designs that incorporate both a GI and an NI system within the same instrument (or one could consider flying both a GI and an NI telescope). One such design is shown in Fig. 3.5.There are two major advantages to this design: 1) it provides the best features of both types of telescope, as discussed above; 2) it provides both a high resolution (NI) and a full Sun (GI) instrument.

The major disadvantages of this design are increased complexity, higher cost and greater risk, due to the number of mechanisms required.

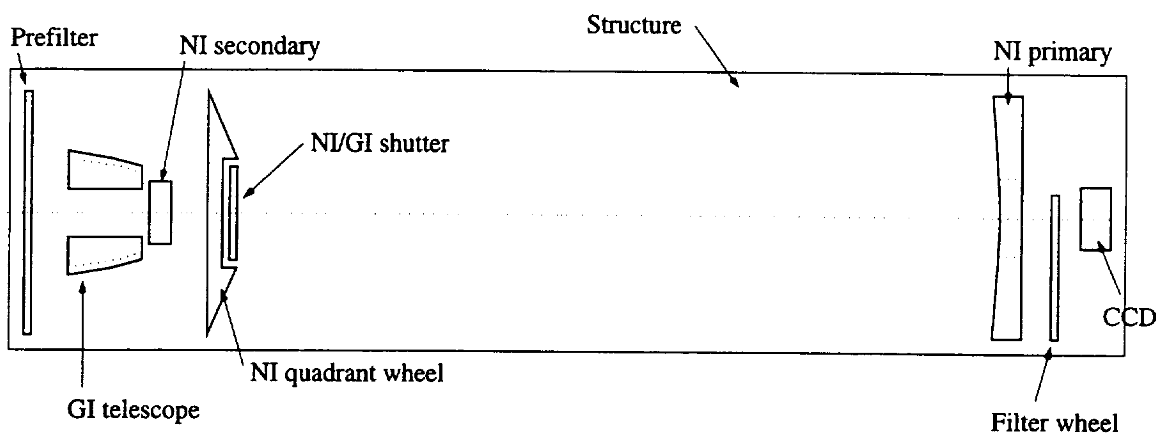

Figure 3.5: Schematic design of the combination GI/NI x-ray telescope.

3.1.6 Tuneable GI Telescope

The standard Wolter I grazing incidence telescope for solar coronal studies is broadband and typically operates in the wavelength region from ~ 3 Å to ~ 60 Å. Temperature diagnostics are performed by inserting various thin film transmission filters into the optical path, thereby narrowing the passband to a narrower portion of the total range. The ratio of two passbands is then temperature-dependent. A number of filters is typically placed on a filter wheel just ahead of the focal plane.

It is also possible to obtain narrow passbands by inserting a flat, multilayer coated mirror (or crystal), which selects a very narrow range of wavelengths from the broad passband. A $\theta - 2\theta$ rotation of the flat mirror and the focal plane detector will then allow the narrow passband to be tuned over a considerable range of wavelengths. Multilayers with moderately high reflectivity ($\sim 30\%$) at grazing angles of 10–20 degrees can provide bandwidths of ≈ 2Å in this spectral region.

This type of instrument provides improved spectral discrimination over standard thin-filter designs. The major disadvantage is the relatively difficult motion of the focal plane detector which is required.

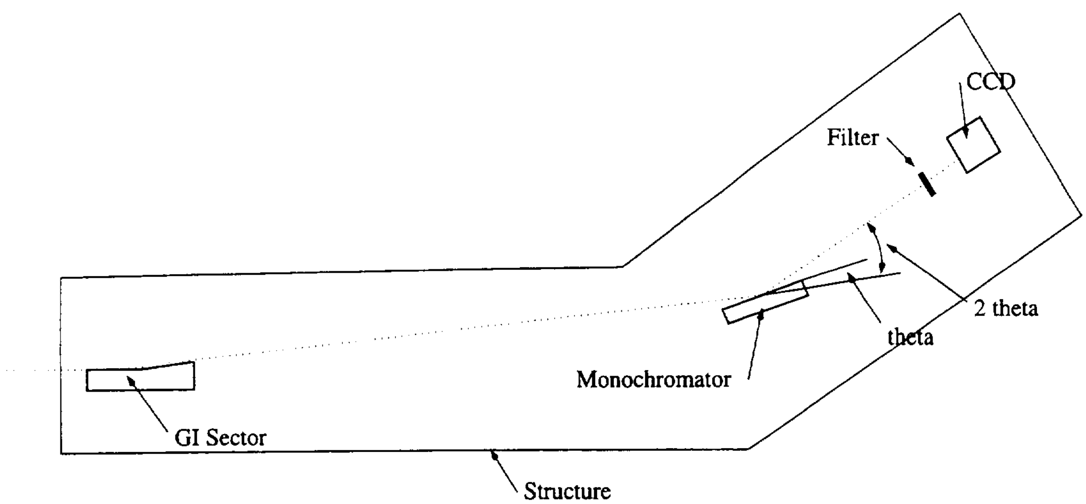

Figure 3.6: Schematic design of the Tuneable GI telescope

4.1 ~~Budgetary Estimate~~